MNRAS 000, 1–15 (2022) Preprint 11 October 2022 Compiled using MNRAS LATEX style file v3.0

Radial and vertical structure of accretion disk around magnetized star

Aleksey Kuzin,[1]★ Galina Lipunova,[1] Danil Lisitsin[1]
[1]1Moscow Lomonosov State University Sternberg Astronomical Institute, Moscow 119992, Universitetskiy pr., 13, Russia

Accepted XXX. Received YYY; in original form ZZZ

ABSTRACT

Accretion disks around magnetized neutron stars reveal themselves in observed X-ray sources. We consider effects of the magnetic field of a central star on a steady accretion disk assuming that magnetic field of a central star can penetrate the disk. We construct an analytical model of disk-magnetic field interaction and calculate how the structure of the accretion disk depends on the magnetic field. To calculate the induced magnetic field, induction equation is examined and some analytical solutions were found. Motion equations are modified taking the magnetic field into account. The inner radius of the accretion disc and the viscous stress tensor follows from the found distribution of the magnetic torque. For low accretion rate, the inner radius can be very different from the Alfven one. A modified system of equations for the vertical structure is solved self-consistently with the induction equation to find radial and vertical distributions of parameters in the disk. In addition, we calculate the spectra of the disk thermal emission. We show that normalized relative vertical structure is basically the same for any set of parameters. Nevertheless, the magnetic field can sufficiently modify the viscous tensor, radial structure, and spectra of the disk.

Key words:
accretion, accretion discs – stars: neutron – . . .

1 INTRODUCTION

Despite a lot of works concerning a behaviour of an accretion disk around magnetized star, there is still a lack of understanding of how the structure of an accretion disk changes in a presence of a strong magnetic field. In the present paper we assume a neutron star (NS) as the central star, since we are interested mostly in the behaviour of the disk during the X-ray outbursts. Nevertheless, the results of this paper can be also applied to the cases of accretion onto the white dwarfs, T-Tauri stars or onto any magnetic and spinning object.

We consider a situation when the magnetic field managed to penetrate the disk. Due to ionized state of the disk the magnetic lines tend to be engaged by the rotating matter, and induced components of the field appear (a dynamo mechanism).

One of the first attempts to build a self-consistent model of accretion disk interacting with magnetic field was the series of works Ghosh et al. (1977) Ghosh & Lamb (1979a), Ghosh & Lamb (1979b). Radial distribution of parameters were found, but the induced magnetic field was set up artificially. Later Wang (1987) showed that the pressure of such induced magnetic field would destroy the disk far from the central star. Another important effect that was not considered by Gosh and Lamb was reconnection of the magnetic field lines: the lines can reconnect in the region : where Keplerian velocity in the disk differs much from the magnetosphere velocity (Lovelace et al. 1995). This process limits the growth of induced magnetic field due to dynamo mechanism.

Campbell & Heptinstall (1998a) and Campbell & Heptinstall (1998b) have built a model for the magnetized accretion disk adopting turbulent diffusivity (buoyancy diffusivity) as a mechanism of magnetic field dissipation. They obtained pretty much the same results in both papers, which is a hint that the exact mechanism of field growth limitation is not important. Campbell (2010) investigated the mechanism of disk disruption near the central star by the magnetic field pressure. This effect is present due to different dependencies of gas pressure and magnetic pressure on the distance to the NS.

The paper is organized as follows. In section 2 we give an overview of the accretion disk model we use. In section 3 we discuss previous models of induced magnetic field and construct our own model. Then we examine closely the equation of angular momentum transport in section 4. The position of the inner radius and the viscous stress tensor are found there. In section 5 we briefly discuss how the presence of a magnetic field affects the blackbody multicolor spectra of the disk. In section 6 we build a model for the vertical structure of the disk, and in the next section 7 the radial structure of the disk is found by solving the system of vertical structure equations at each radius. We discuss our results in section 8.

2 MODEL OF THE DISK

We will use cylindrical coordinates (r, φ, z) everywhere in this work.

We adopt the model of a neutron star with the rotation axis aligned with the accretion disk axis. We assume the magnetic field of the NS to be dipole (the dipole moment of the NS $\mu_m \sim 10^{26} - 10^{27} \mathrm{G \cdot cm^3}$). The inclination angle χ between the magnetic moment $\vec{\mu}_m$ and the angular velocity of the NS $\vec{\Omega}_s$ may be between 0° and 90°.

Our model of an accretion disk and its interaction with the magnetic field is based on a work Kluźniak & Rappaport (2007) (hereafter KR07). Our accretion disk is geometrically thin and optically

★ E-mail: alv.kuzin@gmail.com

thick (relative semi-thickness of the disk $z_0(r)/r \equiv h(r) \ll 1$) and α-prescription for the model of turbulence is adopted. The α-parameter is a free parameter of the model and it is not calculated self-consistently with the magnetic field. The matter is assumed to have a Keplerian angular velocity inside the disk and stellar angular velocity outside the disk.

Following KR07, we assumed that there is an inner radius of viscous accretion disk r_0 on which viscous tensor $W_{r\varphi}$ is zero. There are no viscous torques in the transition region $R_{\max} < r < r_0$ and the motion of matter is controlled only by electromagnetic forces. Here $R_{\max}$ is a maximum of the radius of a neutron star R_s and a radius of the innermost stable circular orbit $R_{\rm ISCO}$: $R_{\max} = \max(R_s, R_{\rm ISCO})$. If we know the magnetic field inside and outside the accretion disk, these assumptions are enough to find the position of an inner radius r_0 and viscous stress tensor $W_{r\varphi}$.

As in KR07, we did not take a Joule heat into consideration and account only for the heat by viscous process since it is not clear which part of Joule heat is released outside the disk.

2.1 Notation

We will use the following notations. Corotation radius is the distance where the Keplerian angular velosity is equal to the stellar one:

$$r_c = \left(\frac{GM_s}{\Omega_s^2}\right)^{1/3}, \tag{1}$$

with Ω_s being the angular velocity oa the NS.

The "light cylinder" radius:

$$r_l = \frac{c}{\Omega_s}. \tag{2}$$

We also introduce $a = r_l/r_c = 4.86 f_{200} M_{1.4}$. The characteristic magnetosphere radius which will be referred as an "Alfven radius":

$$r_a = \left(\frac{\mu_m^2}{\dot{M}\sqrt{GM_s}}\right)^{2/7}. \tag{3}$$

Here $\dot{M}$ is an accretion rate, M_s is a NS mass, μ_m is a magnetic dipole moment of the NS.

The fastness parameter ω is defined as the ratio of a NS angular velocity Ω_s to the Keplerian angular velocity at the distance r_0 :

$$\omega = \frac{\Omega_s}{\Omega_0} = \left(\frac{r_0}{r_c}\right)^{3/2}. \tag{4}$$

Following KR07, let's define the parameter ξ as:

$$\xi = \frac{r_a}{r_c}. \tag{5}$$

This is an estimation of ξ-parameter:

$$\xi = 0.39 \mu_{26}^{4/7} \dot{M}_{17}^{-2/7} M_{1.4}^{-10/21} f_{200}^{2/3}, \tag{6}$$

with the parameters normalized to theirs characteristic values: $\mu_{26} = \mu_m/(10^{26}\ \mathrm{G\cdot cm^3})$, $\dot{M}_{17} = \dot{M}/(10^{17}\ \mathrm{g/s})$, $M_{1.4} = M/1.4M_\odot$, f is a frequency of the NS: $f_{200} = f/(200\ \mathrm{Hz})$. If not specified, $M_{1.4} = 1$, $f_{200} = 1$ everywhere in this work .

2.2 Main equations

Now we will write down the equations of motion which will be used throughout the paper. The Navier-Stokes equations with the magnetic field included:

$$\frac{\partial \vec{v}}{\partial t} + (\vec{v}\nabla)\vec{v} = -\frac{1}{\rho}\nabla\left(P + \frac{B^2}{8\pi}\right) + \frac{1}{4\pi\rho}(\vec{B}\nabla)\vec{B} - \frac{1}{\rho}\nabla\Phi_g + \vec{N}. \tag{7}$$

Here Φ_g is gravitational potential of the NS (we neglect the self-gravity of the disk):

$$\Phi_g = -\frac{GM_s}{\sqrt{r^2+z^2}}, \tag{8}$$

and $\vec{N}$ is a moment of viscous torques in the disk. For the thin disk (see Kato et al. (2008)), if we denote w — is a specific viscous stress tensor:

$$\vec{N} \approx \frac{1}{\rho}\frac{1}{r^2}\frac{\partial}{\partial r}(r^2 w_{r\varphi})\vec{e}_\varphi. \tag{9}$$

The equation of mass continuity:

$$\frac{\partial \rho}{\partial t} + \mathrm{div}(\rho\vec{v}) = 0. \tag{10}$$

Consider the case of a stationary accretion. Then $\frac{\partial}{\partial t} = 0$ and three scalar equations following from the Navier-Stokes equation (7) are:

$$\begin{cases} (\vec{v}\nabla)v_r - \dfrac{v_\phi^2}{r} = -\dfrac{1}{\rho}\dfrac{\partial}{\partial r}\left(P + \dfrac{B^2}{8\pi}\right) + \dfrac{1}{4\pi\rho}\vec{e_r}\cdot(\vec{B}\nabla)\vec{B} - \dfrac{GM_s}{r^2}, \\ (\vec{v}\nabla)v_\phi + \dfrac{v_r v_\phi}{r} = -\dfrac{1}{\rho r}\dfrac{\partial}{\partial \phi}\left(P + \dfrac{B^2}{8\pi}\right) + \dfrac{1}{\rho}\dfrac{\partial}{\partial r}(r^2 w_{r\phi}) + \dfrac{1}{4\pi\rho}\vec{e_\phi}\cdot(\vec{B}\nabla)\vec{B}, \\ (\vec{v}\nabla)v_z = -\dfrac{1}{\rho}\dfrac{\partial}{\partial z}\left(P + \dfrac{B^2}{8\pi}\right) - \dfrac{1}{\rho}\dfrac{GM_s}{r^3}z + \dfrac{1}{4\pi\rho}\vec{e_z}\cdot(\vec{B}\nabla)\vec{B}. \end{cases} \tag{11}$$

We will consider these equations in the following sections of the present paper. Since we suppose disk is axially-symmetric, these equations should be averaged over the φ-angle. For an arbitrary value $x(r,\varphi,z)$ we define:

$$\langle x\rangle_{2\pi} = \frac{1}{2\pi}\int_0^{2\pi} x(r,\phi,z)d\phi. \tag{12}$$

This procedure is justified since the spin period of NS is much greater than the timescales of equilibrium either in vertical or radial direction. The azimuthal equation will also be integrated over z-direction, but we need to specify the magnetic field first. The next section is dedicated to the magnetic field inside the accretion disk.

3 INDUCED MAGNETIC FIELD

In the Wang (1995) author gave the derivation of the induced magnetic field assuming three different machanisms of its dissipation: reconnection of field lines determined by Alfven speed, turbulent diffusion inside the disk, reconnection outside the disk. We are interested in the two last models which will be referred as "diffusion" and "reconnection" models. In the diffusion model the growth of the induced field is "limited by diffusive decay due to turbulent mixing within the disk" and in the reconnection model the azimuthal

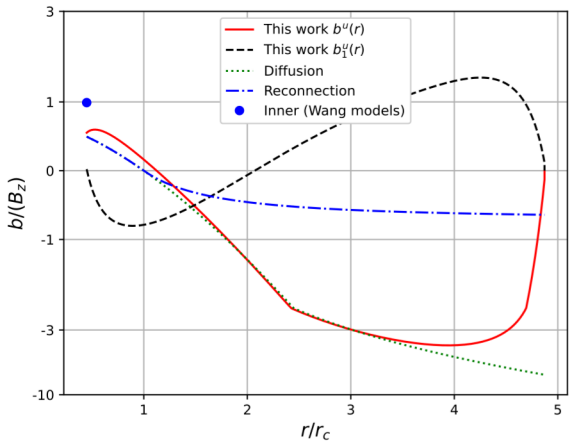

Figure 1. Comparison of magnetic field on the surface of the disk calculated in the present work (components $b^u(r)$ and $b_1^u(r)$) and in models of diffusion and reconnection ($b(r)$ as lines and $b_1(r_0)$ as the dot). Parameter ω is taken to be 0.3 ($r_0/r_c = 0.3^{2/3} \approx 0.45$). Relative thicknesses $h_0 = z_0(r)/r = 0.3$ (for smaller thicknesses b^u is nearly indistinguishable from the diffusion model). Inclination angle $\chi = 45°$. All fields are normalized to the vertical dipole field in the equatorial plane $B_z = \mu/r^3$.

pitch $|B_\varphi/B_z|$ is assumed to be of order unity. Let us introduce two parametrisations of an induced magnetic field ("upper" implies the surface of the disk, "inner" indicates the inner edge of a viscous disk and "inside" means inside the disk):

$$b_\varphi^I = \begin{cases} \Gamma\left(1-\frac{\Omega_k}{\Omega_s}\right)B_z & \text{upper}, z=z_0, \\ -\Gamma\left(1-\frac{\Omega_k}{\Omega_s}\right)B_r & \text{inner}, r=r_0, \\ 0, & \text{inside}. \end{cases} \tag{13}$$

$$b_\varphi^{II} = \begin{cases} -\Gamma\left(1-\frac{\Omega_s}{\Omega_k}\right)B_z & \text{upper}, z=z_0, \\ \Gamma\left(1-\frac{\Omega_s}{\Omega_k}\right)B_r & \text{inner}, r=r_0, \\ 0, & \text{inside}. \end{cases} \tag{14}$$

In Wang's works the magnetic field is specified at the inner radius ("inner") and at the surfaces of the disk ("upper" at the upper surface and minus "upper" at the lower surface). The field inside the disk is assumed to be 0. Here Γ is an unknown dynamo coefficient of order unity. Since we do not have a chance to know this coefficient and to make our life easier, we will ignore this coefficient henceforth. With this notation we write down the Wang's diffusion and reconnection models:

$$b_\varphi^{\text{diff}} = b^{II}, \tag{15}$$

$$b_\varphi^{\text{rec}} = \begin{cases} b_\varphi^{II} & r < r_c, \\ b_\varphi^I & r > r_c. \end{cases} \tag{16}$$

Our aim here is to derive the equation for the induced magnetic field inside and around the disk and then solve it either analytically or numerically. The total magnetic field in our model is the sum of dipole field of a NS and some additional (induced) field which we assume to be a non-zero only in azimuth direction:

$$\vec{B} = \vec{B}_s^{\text{dipole}} + b_\varphi \vec{e}_\varphi = B_r\vec{e}_r + (B_{\varphi 0} + b_\varphi)\vec{e}_\varphi + B_z\vec{e}_z. \tag{17}$$

To derive the general form of an induction equation, we take Maxwell equations and Ohm law:

$$\begin{cases} \text{rot}\vec{B} = \frac{4\pi}{c}\vec{j} + \frac{1}{c}\frac{\partial\vec{E}}{\partial t}, \\ \text{rot}\vec{E} = -\frac{1}{c}\frac{\partial\vec{B}}{\partial t}, \\ \text{div}\vec{B} = 0, \\ \vec{j} = \sigma(\vec{E} + \frac{1}{c}[\vec{v}\times\vec{B}]). \end{cases} \tag{18}$$

Here σ and v are plasma conductivity and velocity. Then we denote $\eta = c^2/4\pi\sigma$. We will assume that this coefficient, magnetic diffusivity, is of turbulent nature (see Campbell (1992) for a justification). Applying $\vec{\nabla}\times$ to the first equation in (18) and using other three equations, we get:

$$\frac{\eta_T}{c^2}\frac{\partial^2\vec{B}}{\partial t^2} + \frac{\partial\vec{B}}{\partial t} = \eta_T\Delta\vec{B} + \text{rot}[\vec{v}\times\vec{B}] + \left[\frac{\text{grad}\eta_T}{\eta_T}\times[\vec{v}\times\vec{B}]\right]. \tag{19}$$

The first term in (19) can be neglected (**should i explain?**). We take the velocity of matter in form:

$$V = \begin{cases} \left(\frac{GM}{r}\right)^{1/2}, & \text{inside the disk}, \\ \Omega_s r, & \text{in the magnetosphere}. \end{cases} \tag{20}$$

and magneric diffusivity in form:

$$\eta_T = \begin{cases} \epsilon_d \nu_T, & \text{inside the disk}, \\ \epsilon_m \nu_T, & \text{in the magnetosphere}. \end{cases} \tag{21}$$

Here η_T is a coefficient of turbulent diffusivity:

$$\nu_T = \frac{2}{3\Pi_1}\alpha\left(\frac{z_0}{r}\right)^2\sqrt{GMr} = 2\cdot10^{13}\left(\frac{\Pi_1}{6}\right)^{-1}\left(\frac{z_0/r}{0.1}\right)^2\alpha_{0.5}r_7^{1/2}M_{1.4}^{1/2}. \tag{22}$$

Here Π_1 is a dimensionless parameter ($\Pi_1 \approx 6-7$) that can be calculated for the each radius after the vertical structure is found (see 6). This parameter depends extremely weakly on the distance r.

We will find ϵ_d from the condition that the induced magnetic field should be consisted with the Wang's "diffusion" model (15). As for the coefficient ϵ_m, for this work it is enough to suppose $\epsilon_m/\epsilon_d \gg 1$. We will assume the following form for the induced field:

$$b_\varphi = b(r,z) + b_1(r,z)\cos\varphi + b_2(r,z)\sin\varphi. \tag{23}$$

It will be shown in Appendix A that there are no other components of induced field. The boundary conditions at the inner radius and at the surfaces of the disk follow from the equation itself, but one have to set another condition. We set zero condition on the light cylinder $r_l = c/\Omega_s$ for the induced field. Let us denote: $r_l = ar_c$. In the main body of the paper we have no intend to investigate the components b_1 and b_2 in the equations, so now we will discuss only the equation for the b (see Appendix A for the detailed derivation of this equation as well as the equations fot b_1 and b_2):

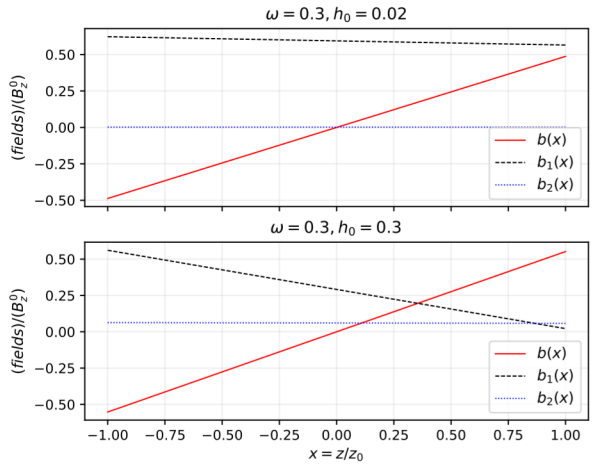

Figure 2. Vertical structure of a magnetic field. Parameter ω is taken to be 0.3 ($r_0/r_c = 0.3^{2/3} \approx 0.45$). Field evaluated at the inner radius of the disk. Two different relative thicknesses $h_0 = z_0(r)/r$ are shown: $h_0 = 0.02$ for the upper picture and $h_0 = 0.3$ for the lower picture. Inclination angle $\chi = 45°$. Notice that $b(x)$ is the anti-symmetric function, while $b_1(x)$ is nearly constant with $h_0 \ll 1$ and linear function with $h_0 \sim 1$. All fields are normalized to the vertical dipole field in equatorial plane at the inner radius $B_z^0 = \mu/r_0^3$.

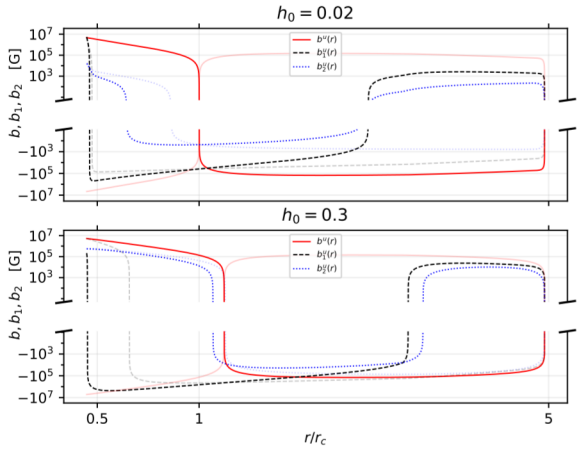

Figure 3. Magnetic field on the surface of the disk calculated in the present work, to the distance to central NS (in units of corotation radius). Parameter ω is taken to be 0.3 ($r_0/r_c = 0.3^{2/3} \approx 0.45$). Fields were evaluated at the upper surface (bright lines) and lower surface (pale lines) of the disk. Two different relative thicknesses $h_0 = z_0(r)/r$ are shown: $h_0 = 0.02$ for the upper picture and $h_0 = 0.3$. Inclination angle $\chi = 45°$.

$$\begin{cases} \dfrac{1}{r}\dfrac{\partial}{\partial r}\left(r\dfrac{\partial b}{\partial r}\right) - \dfrac{b}{r^2} + \dfrac{\partial^2 b}{\partial z^2} = 3C\dfrac{z}{r^6}, \\ \left.\dfrac{\partial b}{\partial z}\right|_{z=z_0} = \left.\dfrac{\partial b}{\partial z}\right|_{z=-z_0} = \dfrac{C}{2}\dfrac{1}{r^4}\left(1 - \dfrac{\Omega_s}{\Omega_k}\right), \\ \left.\dfrac{\partial b}{\partial r}\right|_{r=r_0} = -\dfrac{3C}{2r_0^5}(1-\omega)z, \\ b(r = r_l) = 0. \end{cases} \tag{24}$$

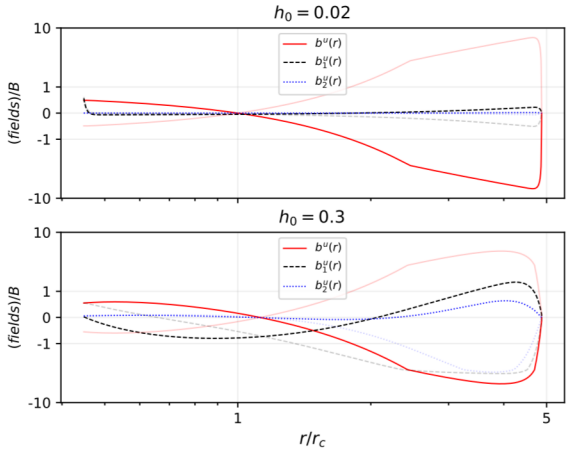

Figure 4. The same as at the Figure 3, but all the fields are normalized to the vertical dipole field at the equator $B_z = \mu/r^3$. Parameter ω is taken to be 0.3 ($r_0/r_c = 0.3^{2/3} \approx 0.45$). Fields were evaluated at the upper surface (bright lines) and lower surface (pale lines) of the disk. Two different relative thicknesses $h_0 = z_0(r)/r$ are shown: $h_0 = 0.02$ for the upper picture and $h_0 = 0.3$. Inclination angle $\chi = 45°$.

Here $C = 3\Pi_1 \mu \cos\chi / 2\alpha h^2 \epsilon_d$. To reset the conditions upon z-axis and to determine ϵ_d, we perform the trick:

$$b(r,z) = \frac{C}{2}\frac{z}{r^4}\left(1 - \frac{\Omega_s}{\Omega_k}\right) + \beta(r,z) = b_0(r,z) + \beta(r,z). \tag{25}$$

We get the following boundary condition problem for the $y(r,z)$:

$$\begin{cases} \dfrac{1}{r}\dfrac{\partial}{\partial r}\left(r\dfrac{\partial \beta}{\partial r}\right) - \dfrac{\beta}{r^2} + \dfrac{\partial^2 \beta}{\partial z^2} = \dfrac{3C}{2}\dfrac{z}{r^6}\left(\dfrac{7}{4}\dfrac{\Omega_s}{\Omega_k} - 3\right), \\ \left.\dfrac{\partial \beta}{\partial z}\right|_{z=z_0(r)} = \left.\dfrac{\partial \beta}{\partial z}\right|_{z=-z_0(r)} = 0, \\ \left.\dfrac{\partial \beta}{\partial r}\right|_{r=r_0} = \dfrac{C}{2r_0^5}(1+\omega/2)z, \\ \beta(r = r_l) = -\dfrac{C}{2}\dfrac{z}{r_c^4}\dfrac{1 - a^{3/2}}{a^4}, \end{cases} \tag{26}$$

Wang's diffusion and reconnection models of an induced magnetic field are shown at Figure 1 along with the magnetic field obtained in the current work (all the fields are evaluated at the upper surface of the disk). We clearly see that the curve for our model is close to the diffusion model everywhere except for the regions near the boundaries of the $[r_0, r_l]$ line segment. This is not surprising since the same mechanism for limiting the growth of the magnetic field is adopted in both the diffusion model and our work. In opposite, the black dashed line that indicates the component proportional to $\cos\varphi$ are far away from the blue dot denoting the Wang's field at the inner edge of the disk. It shows the importance of fair b_r calculation rather than order-of-magnitude estimates.

The analytical solution for this problem is given in Appendix B. It is easy to see that magnetic field b is dominated by b_0, and β is just a small correction from the boundary conditions. Thus, for the purpose of matching our solution with Wang's diffusion model, we will require in $r \in [r_0, r_l]$ $b_0(z = z_0) = b_\varphi^{\rm diff}$, or $C = 2\mu\cos\chi/h_0$. This implies $\epsilon_d = 3\Pi_1/4\alpha h$. We notice that this coefficient is large.

Since we found the analytical solution for this problem, it is not

necessary for us to solve it numerically. Nevertheless, we describe the easy way to reduce it to one-dimensional equation which can be easily solved. This is important for the problem for b_1 and b_2. We expand the solution in series $\beta = \sum_n Z_n(z)R_n(r)$, where $Z_n(z)$ are eigenfunctions of the problem

$$\begin{cases} Z_n'' + \mu_n^2 Z_n = 0, \\ Z_n'(z_0) = Z_n'(-z_0) = 0. \end{cases} \tag{27}$$

The solutions are $\sin \pi(n+1/2)z/z_0, \mu_n = \pi(n+1/2)/z_0$ and $\cos \pi n z/z_0, \mu_n = \pi n/z_0$, n varies in range $0, 1, ... + \infty$. Since in our particular case the function is anti-symmetric, there are no contributions from consines. For the problem of b_1, b_2 there is also a contribution from $\cos(0 \cdot z/z_0) = 1$.

Vertical structure of the induced magnetic field evaluated at the inner edge of the viscous disk is shown at the Figure 2. Two main conclusions should be derived from the results at this figure. First, the component b is (with a great precision) an anti-symmetrical function of z-coordinate. Second, the component b_1 at the inner radius is nearly a constant, if the disk is thin, and linear function, if the thin disk assumption is not satisfied. Also, the component b_2 is sufficiently smaller than b and b_1 for any adequate set of parameters ω, h_0, χ.

The radial structure of the induced magnetic field is shown at the Figures 3 (in absolute values) and 4 (normalized to the dipole field). Notice that as relative half-thickness becomes larger, the importance of b_1 and b_2 over b grows. For example, when $h_0 = 0.02$, the b_1 component is significant only near the inner edge of the disk, but when $h_0 = 0.3$, both b_1 and b_2 are comparable with b. Thus, to calculate the heat release or the structure of the disk with strong magnetic field penetrated the disk, one should account for all the components of the induced field.

4 ANGULAR MOMENTUM TRANSPORT

Our aim in this section is to examine the equation of the angular momentum transport (the second one in the eq. (11)). There are two main purposes for that. First, the equation for the inner radius of the viscous disk can be found from the equation of angular momentum transport. In the work Revnivtsev et al. (2009) the position of the inner radius of the accretion disk around NS was traced throughout the X-ray outburst (see further in the text for the details). Even though the inner radius in this work was model-dependent, this work shows the possibility of comparison of the model for the inner radius with phenomena observed in nature.

The second purpose of this section is to derive the expression for the viscous stress tensor $W_{r\phi}$. Once this is done, the heat generation due to viscous processes could be calculated. The heat release rate in the disk is the key moment for calculation of vertical and radial profiles of all parameters of the disk.

4.1 General equations

For the derivation of the next equation we also use the approximation $h_0(r) = z_0(r)/r_0 \approx$ const and the explicit form of the dipole magnetic field (A2). The angular velocity is assumed to be Keplerian everywhere. We now take the second equation of the system (11), average it over $\varphi \in [0, 2\pi]$ and integrate over $z \in [-z_0, z_0]$:

$$-\dot{M}\frac{d(\Omega r^2)}{dr} = 2\pi\frac{d}{dr}(r^2 W_{r\phi}) + \frac{1}{2}\int_{-z_0}^{z_0}\frac{d}{dr}\langle r^2 B_\varphi B_r\rangle \mathrm{d}z + \\ + r^2\langle B_z B_\phi\rangle\Big|_{z=-z_0}^{z=z_0}. \tag{28}$$

In this equation we neglect all terms proportional to the power of $h = z_0/r$ higher than 1. In *all* work all such terms will be neglected. This is due to our thin disk approximation. If the thin disk condition is not met, the much bigger problems will arise: non-keplerian rotation, non-locality of pressure and radiative flux (vertical and radial equations will not divide).

This equation was obtained in Wang (1997). The way in which one can get the algebraic equation for the inner radius was shown in Bozzo et al. (2018) (Wang presented the equation earlier, but did not report how it was obtained and what the solutions are). It is seems like in both works the authors have not considered the proper expression for the dipole magnetic field. As a result, some terms in the final equations was missing. It easily can be seen from the equation (26) that the field $b(r, z)$ is the anti-symmetric function of z. Thus one can write $b(z = z_0) = -b(z = -z_0)$. The integral of the b over $[-z_0, z_0]$ is zero.

From the numerical solutions of the equations for b_1, b_2 follows that $b_1(z)$ is not only *not*-anti-symmetric, but rather a constant over all the interval $[-z_0, z_0]$ near the inner radius r_0. Thus we can write $b_1(r_0, z_0) = b_1(r_0, -z_0)$ and $\int_{-z_0}^{z_0} b_1(r_0, z)\mathrm{d}z \approx 2z_0 b_1(r_0, 0)$. In opposite, $b_1(z)$ becomes nearly-anti-symmetric far away from the inner edge of the disk. Taking the induced magnetic field in a form (23) and the dipole field of the NS as in the equation (A2), we get from the last equation (28):

$$-\dot{M}\frac{d(\Omega r^2)}{dr} = 2\pi\frac{d}{dr}(r^2 W_{r\phi}) + \frac{\mu}{2}\sin\chi\int_{-z_0}^{z_0}\frac{d}{dr}\left(\frac{b_1}{r}\right)\mathrm{d}z + \\ + \frac{\mu}{2r}(-b\cos\chi + \frac{3}{2}b_1 h\sin\chi)\Big|_{z=-z_0}^{z=z_0}. \tag{29}$$

This is the most general (with the assumptions made) equation of motion of the matter in the disk. If one sets the inner conditions for the viscous torque, the position of the inner radius can be found (see the next subsection). If the inner condition for the viscous stress tensor is set at the inner radius, the viscous tensor itself can be found.

4.2 Inner radius

Now, to obtain the equation for the inner radius of the viscous disk, we want to do several steps.

There are works **(chashkina, ???)** where the authors assume some external torques act on the inner edge of the disk. Instead, to make live easier, we require quasi-standard condition to be satisfied at the inner edge:

$$W_{r\varphi}\Big|_{r=r_0-0} = 0. \tag{30}$$

It will be shown that at the distances $r > 2 - 3r_0$ this model is actually very similar to the ones described above and it also allows to calculate the effective "torque at the inner edge" that would give the similar results. This condition is not important for the calculation of the inner radius, but will be used as an initial condition for the $W_{r\varphi}$.

Another condition at the inner edge is required. We suppose that the viscous torque at the inner edge is also zero:

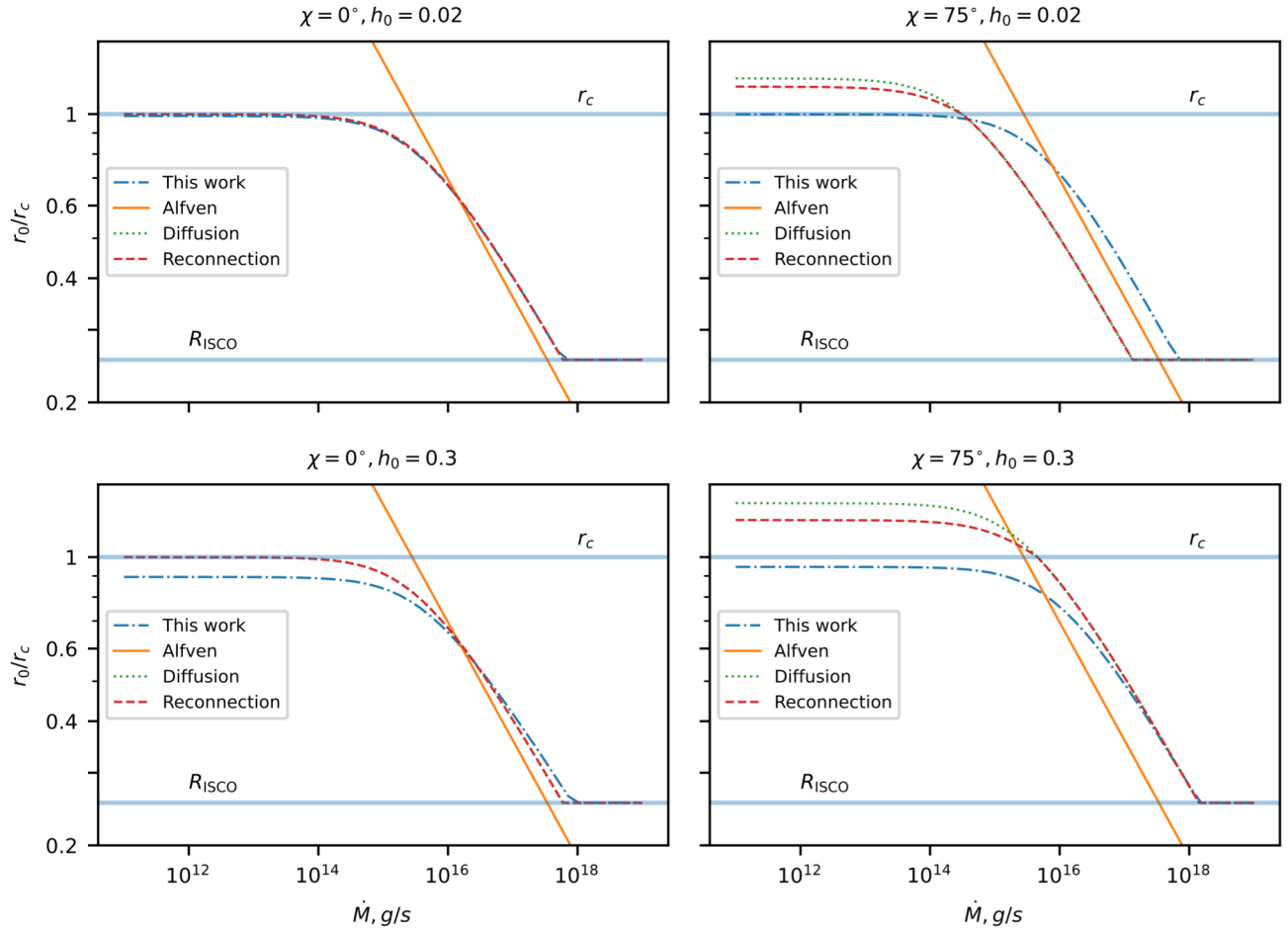

Figure 5. Dependence of the position of the inner radius of a viscous accretion disk (in units of corotation radius) on the accretion rate $\dot{M}$. Magnetic dipole moment is fixed at $\mu = 10^{26} G \cdot cm^3$.

$$\left.\frac{d(r^2 W_{r\varphi})}{dr}\right|_{r=r_0} = 0. \tag{31}$$

With these conditions the equation (29) yields the equation for the inner radius of viscous disk r_0. With all being said about the magnetic field behaviour near the inner edge of the disk, we rewrite the general equation (29) as follows (we denote the quantities x on the surface of the disk as x^u):

$$\frac{1}{2}\frac{\dot{M}\sqrt{GMr_0}}{\mu} = b^u(r_0)\cos\chi - \frac{z_0}{r_0}r_0^2\frac{d}{dr}\left(\frac{b_1}{r}\right)\Big|_{r_0,0}\sin\chi. \tag{32}$$

Now all we should do is specify the model for the induced magnetic field. For parametrizations I (13) and II (14) we obtain:

$$\begin{cases} 1/2 = \xi^{7/2}\omega^{-10/3}\left[(1-\omega)\cos^2\chi - h_0(8\omega-11)\sin^2\chi\right], & \text{param. I,} \\ 1/2 = \xi^{7/2}\omega^{-7/3}\left[(1-\omega)\cos^2\chi - h_0(5\omega-8)\sin^2\chi\right], & \text{param. II.} \end{cases} \tag{33}$$

The inner radius $r_0 = r_c \cdot \omega^{2/3}$, where ω for Wang's diffusion and reconnection models are:

$$\begin{cases} \omega^{\rm diff} = \text{solution for param. II,} \\ \omega^{\rm rec} = \begin{cases} \text{solution for param. II if } \omega < 1, \\ \text{solution for param. I if } \omega < 1. \end{cases} \end{cases} \tag{34}$$

The real inner radius is calculated as $r_{in} = \max(r_0, R_{\rm max})$ with $R_{\rm max} = \max(R_{\rm ISCO}, R_s)$. We will denote the real inner radius r_{in} as r_0 anyway.

At the Figure 5 we show the inner radius dependence on the accretion rate for the diffusion and reconnection models of the magnetic field (solutions of (34)) and for our model (solution of the general equation (32)). The "Alfven" curve indicates the inner radius calculated as $r_0 = (\mu^4/\dot{M}^2 GM)^{1/7}$. All three models of the induced magnetic field are close to "Alfven" curve when the accretion rate is high. When the accretion rate is weak, though, all models show that the inner radius would not increase unlimited, as in "Alfven" model, but would limited by some value. In case of inclination angle $\chi = 0$ and $h_0 \ll 1$, this value is corotation radius: $r_0 < r_c$. This was shown in Bozzo et al. (2018) already. It worth to mention that this limit can exceed the corotation radius in case of $\chi \neq 0$. In the case

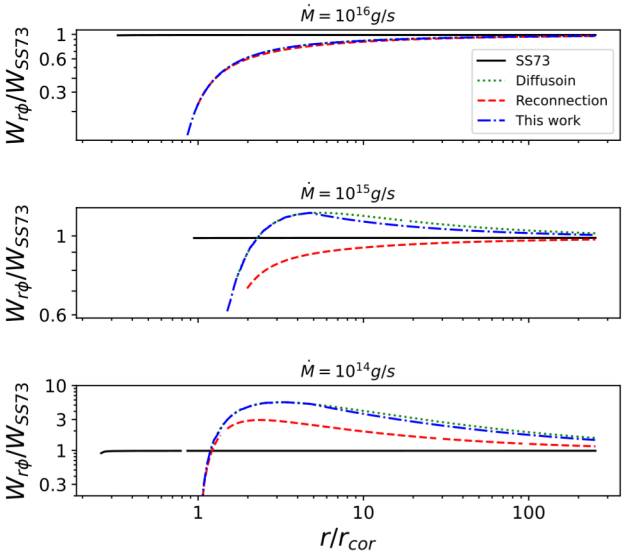

Figure 6. The viscous stress tensor as a function of distance to the NS (in units of corotation radius) for different models of induced magnetic field. $\chi = 0$. $\mu = 10^{26} G \cdot cm^3$.

of our model the inner radius cannot exceed the corotation radius significantly.

4.3 Viscous stress tensor

Now having the inner radius r_0, one can calculate the viscous stress tensor.We will denote the parameters onto the surface of the disk with the index ^{u}, e.g., the induced field at the $z = z_0$ is b^u_φ. We also introduce $I_z(r)$: $b_1(r, z)$ integrated over the z-coordinate, $I_z(r) = \int_{-z_0}^{z_0} b_1(r, z)\mathrm{d}z$. From the equation of angular momentum transport (29) we can obtain:

$$W_{r\varphi} = -\frac{\dot{M}\Omega_k}{2\pi}\left(1 - \sqrt{\frac{r_0}{r}}\right) + \frac{\mu\cos\chi}{2\pi r^2}\int_{r_0}^{r}\frac{b^u(\rho)}{\rho}\mathrm{d}\rho - \\ - \frac{3}{2}\frac{\mu h\sin\chi}{2\pi r^2}\int_{r_0}^{r}\frac{b^u_1(\rho)}{\rho}\mathrm{d}\rho - \frac{\mu\sin\chi}{2}\left(\frac{I_z(r)}{r} - \frac{I_z(r_0)}{r_0}\right). \quad (35)$$

Let us consider the diffusion and reconnection models. In these models we assume b_1 to exist only on the inner radius, i.e., $b_1(r) = b_1^{\mathrm{inner}}$ if $r = r_0$ and $b_1(r) = 0$ elsewhere. This is, of course, an oversimplification, but numerical results of the present paper show that the assumptions mentioned above are probably not far from truth. We do not give the expressions for viscous tensor with these models of induced magnetic field due to cumbersomeness of the formulas. In the Figure 6 the comparison between viscous tensors in these models and in our model of magnetic field is shown. We can see that when the accretion rate is high, the absolute value of a viscous tensor is smaller that the one without the magnetic field. Indeed, the inner radius of the viscous disk is bigger than R_{ISCO} because of the magnetic field pressure, but the energy release due to magnetic field is still small. As the accretion rate decreases, the relative impact of the magnetic field into the energy release increases and even becomes larger than in the standard disk model.

5 SPECTRA OF THE DISK

In this section we show how the spectra of the disk changes with the presence of the strong magnetic field (of with small accretion rate). We want to emphasize that there is no proper spectra modelling in this paper. We apply the black-body radiation model, and all results of this section only show that the spectra of the disk around magnetized star can differ from the spectra of the disk around the black hole.

The viscous tensor (35) depends on the relative half-thickness of the disk h_0 which is to be found. Nevertheless, in the following sections it will be shown that $h_0(r)$ is very weak function of r and thus can be approximated by constant value; also we will find that $h_0 = 0.02$ for the standard disk and $h_0 = 0.06$ for the strongly magnetized disk are good approximations. We will use them in this section.

One can calculate the radiation flux from the surface of the disk:

$$Q_0 = \frac{1}{2}W_{r\phi}r\frac{d\Omega_k}{dr}, \quad (36)$$

and the effective surface temperature using Stephan-Boltzmann law with the constant σ_b:

$$T_{eff} = (Q_0/\sigma_b)^{1/4}. \quad (37)$$

In isothermal atmosphere without the scattering the Planck spectrum is formed:

$$I_\nu = B_\nu^{\mathrm{Planc}} = \frac{2h\nu^3}{c^2}\frac{1}{\exp(h\nu/kT) - 1}. \quad (38)$$

Let d will be the distance to the system and $\cos i$is the cosine of the inclination angle (angle between the disk axis and the line of sight):

$$\frac{F(\nu)d^2}{\cos i} = 2\pi\int_{r_{in}}^{r_{out}} I_\nu r dr. \quad (39)$$

It can easily be shown that the **intermediate** asymptotic ($\nu_0 \ll 1$ and $\nu_0(r_{out}/r_0)^{3/4} \gg 1$) for the spectra are $F(\nu) \propto \nu^{1/3}$ for the weak magnetic field or big accretion rate and $F(\nu) \sim \nu^{5/7}$ for the strong magnetic field or weak accretion.

The results of blackbody spectrum calculation are shown at the figure 7. As the accretion rate decreases, the relative contribution of the magnetic field into the energy release increases. When the accretion rate is weak (or the magnetic field is strong!), spectrum can be significantly different from the one in standard model of accretion.

6 VERTICAL STRUCTURE

Now the vertical structure can be calculated. We use the method similar to that of Π-parameters introduced in Ketsaris & Shakura (1998). The advantage of this method is that the radial structure can easily be calculated after the computation of the vertical structure on the each radius. This method also allows to make an analytical analysis of the results. Since we want to solve the first kind boundary value problem with only one eigenvalue, not four, we modified this method.

6.1 Main equations

We will use the model of ideal gas:

$$P = \frac{\rho\Re T}{\mu}, \quad (40)$$

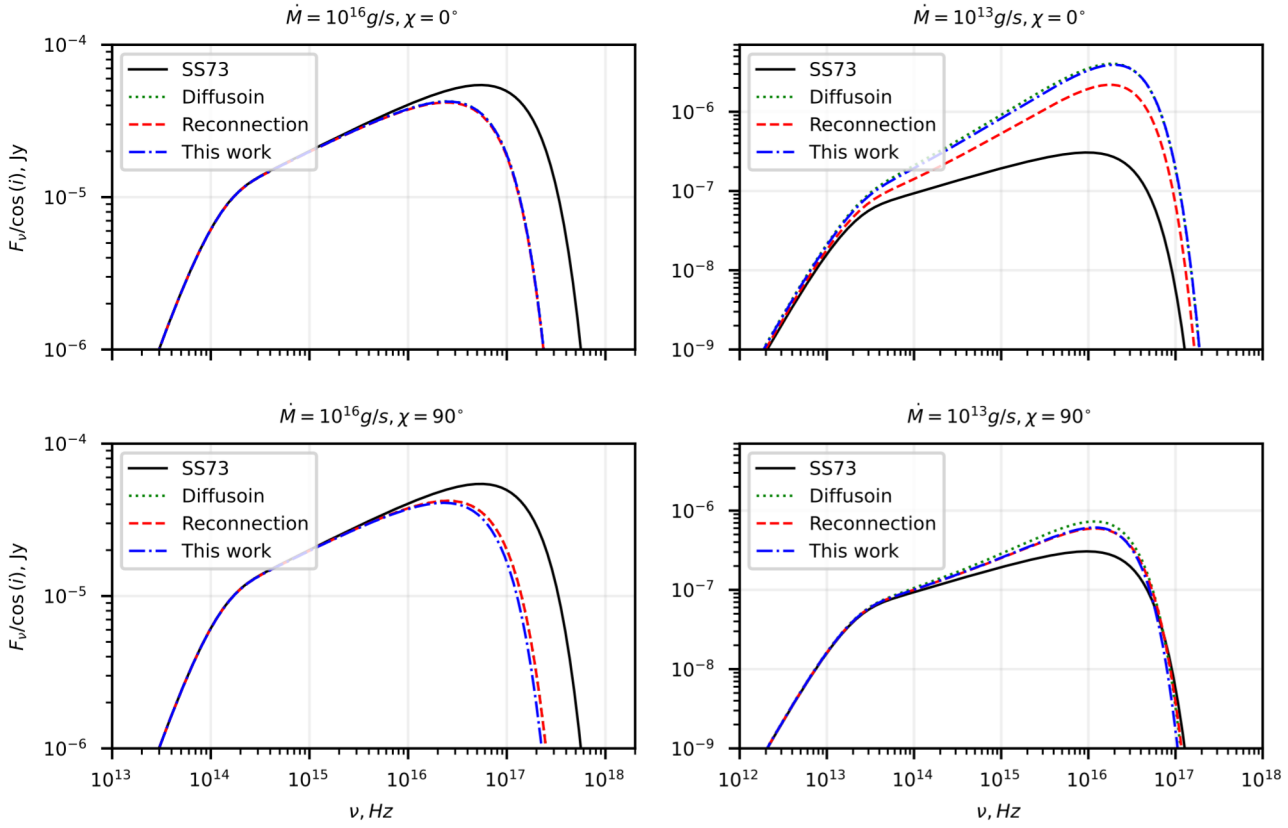

Figure 7. Blackbody spectra of the disk for different accretion rates $\dot{M} = 10^{16} g/s$ (usual for the peak of the X-ray outburst, left column) and $\dot{M} = 10^{13} g/s$ (usual for the plateau of the X-ray outburst, right column). Different inclinations $\chi = 0^\circ, \chi = 60^\circ$ are considered. $\mu = 10^{26} G \cdot cm^3$.

and $\mu = 0.6$ is assumed everywhere. First, let us take the equation of the vertical hydromagnetic equilibrium (last equation in (11)) and average it over $\varphi \in [0, 2\pi]$. It yields:

$$\frac{\partial}{\partial z}\left(P + \frac{B^2}{8\pi}\right) = -\rho\Omega_k^2 z + \frac{1}{4\pi}(\vec{B}\nabla)B_z. \tag{41}$$

With a bunch of boring mathematics it becomes:

$$\frac{\partial P}{\partial z} = -\rho\Omega_k^2 z - \frac{1}{8\pi}\frac{\partial}{\partial z}\left(b^2 + \frac{b_1^2 + b_2^2}{2}\right) - \frac{\mu \sin\chi}{8\pi r^3}\frac{\partial b_2}{\partial z}. \tag{42}$$

For our conveniance we introduce the "magnetic gradient" which is essentially all the effects from the magnetic field:

$$\left(\frac{\partial P}{\partial z}\right)_{\rm m} = -\frac{1}{8\pi}\frac{\partial}{\partial z}\left(b^2 + \frac{b_1^2 + b_2^2}{2}\right) - \frac{\mu \sin\chi}{8\pi r^3}\frac{\partial b_2}{\partial z}. \tag{43}$$

Q is the radiative flux along the z-axis. Let $\epsilon_{rad} = aT^4$ be the radiation energy density ($a = 4\sigma_b/c$). If one neglects all the mechanisms of the heat transfer except for the radiative one, the equation of the heat transfer is:

$$Q = -\frac{c}{3\kappa_R \rho}\frac{d\epsilon_{rad}}{dz}. \tag{44}$$

Here $r\kappa_R$ is Rosseland mean opacity. We will consider the analytical opacity:

$$\kappa_R = \kappa_0 \frac{\rho^\iota}{T^\gamma}. \tag{45}$$

If the opacity is determined by the electron scattering, $\kappa_R = \sigma_t$ — Thompson opacity, $\iota = \gamma = 0, \kappa_0 = \sigma_t = 0.335$ cm^2/g for the solar **abundance**. If the opacity is determined by the bremsstrahlung, $\iota = 1, \gamma = 7/2, \kappa_0 = 5 \cdot 10^{24}$ cm^5 $K^{7/2}$ g^{-2} — Kramers opacity. (see, e.g., Lipunova et al. 2018 Lipunova et al. (2018)).

We also introduce $\Sigma(z)$ as a mass coordinate:

$$\Sigma = \int_0^{z_0} \rho(z_1) dz_1, \tag{46}$$

and $2\Sigma(z_0(r))$ is the disk surface density at the distance r from the NS. The full system of equations for the vertical structure then:

$$\begin{cases} \dfrac{\partial P}{\partial z} = -\rho\Omega_k^2 z + \left(\dfrac{\partial P}{\partial z}\right)_{\rm m}, \\ \dfrac{d\Sigma}{dz} = -\rho, \\ \dfrac{c}{3\kappa_R\rho}\dfrac{d(aT^4)}{dz} = -Q, \\ \dfrac{dQ}{dz} = -w_{r\phi} r \dfrac{d\Omega_k}{dr} = \dfrac{3}{2}\Omega_k \alpha P. \end{cases} \tag{47}$$

Now we normalize all quantities: $P = p \cdot P_0, T = \theta \cdot T_0, \Sigma = \sigma \cdot \Sigma_0/2, Q = q \cdot Q_0$, $z = z_0(1-\zeta)$. $\zeta = 0(1)$ corresponds to the surface (equator) of the disk. Note that these are not a normalizations to the values in the disk equator as in Ketsaris & Shakura (1998). Instead, we choose these values as follows: Q_0 is the same as in (36), $P_0 = \frac{2Q_0}{3\alpha\Omega_k z_0}$, $T_0 = \frac{\Omega_k^2 z_0^2 \mu}{\Re}$, $\Sigma_0 = \frac{2P_0\mu z_0}{\Re T_0}$. For the dimensionless quantities the equation (47) takes the form:

$$\begin{cases} \frac{dp}{d\zeta} = \frac{p}{\theta}(1-\zeta) - \frac{z_0}{P_0}\left(\frac{\partial P}{\partial z}\right)_{\mathrm{m}}, \\ \frac{d\sigma}{d\zeta} = \frac{p}{\theta}, \\ \frac{d\theta}{d\zeta} = \mathcal{K}\frac{qp^{\iota+1}}{\theta^{\iota+\gamma+4}}, \\ \frac{dq}{d\zeta} = -p, \end{cases} \tag{48}$$

with

$$\mathcal{K} = \frac{3}{4}\frac{Q_0\kappa_0 P_0^{\iota+1}\mu^{\iota+1}z_0}{ac\Re^{\iota+1}T_0^{\iota+\gamma+5}}. \tag{49}$$

For a given r coefficient $\mathcal{K}$ depends only on the disk height z_0. The system (48) should be integrated from $\zeta = 0$ (surface of the disk) to $\zeta = 1$ (the equator plane). If four initial conditions onto a surface of the disk and one boundary condition in the disk plane are set, one can calculate the distribution of dimensionless quantities p, q, σ, θ and determine the disk height z_0.

6.2 Boundary and initial conditions

The optical thickness will be **counted** from outside to the inside of the disk:

$$\tau(z) = -\int_{\infty}^{z} \kappa_R \rho dz. \tag{50}$$

To jointly account for the effects of scattering and absorption, the effective optical thickness is introduced (Zel'dovich & Shakura (1969)):

$$\tau_{eff}(z) = -\int_{\infty}^{z} \sqrt{\kappa_{abs}(\kappa_{sc}+\kappa_{abs})}\rho dz, \tag{51}$$

or

$$\frac{d\tau_{eff}}{d\tau} = \sqrt{\frac{\kappa_{abs}}{\kappa_{abs}+\kappa_{sc}}}. \tag{52}$$

with $\kappa_{abs}, \kappa_{sc}$ are opacity coefficients by absorption and scattering.

We use the Eddington approximation for the temperature in the photosphere of the disk:

$$T = T_{eff}\cdot\left(\frac{1}{2}+\frac{3\tau}{4}\right)^{1/4}. \tag{53}$$

The surface of the disk if defined as the height at which the effective optical thickness $\tau_{eff} = 2/3$.

Now we have to understand the behaviour of the pressure $P(\tau)$ in the photosphere. This step is sufficient to define the initial condition for pressure as well as for the searching for the τ. Consider the equation (42). Then multiply it byκ^{-1} and notice that $\kappa\rho dz = -d\tau$:

$$\frac{dP}{d\tau} = \frac{z_0\Omega_k^2}{\kappa} - \frac{1}{\kappa\rho}\left(\frac{\partial P}{\partial z}\right)_m. \tag{54}$$

The vertical coordinate is assumed to change insignificantly while $\tau_{eff} = 2/3$ is accumulated, so $z \approx z_0$. Using (53), equation (54) can be integrated over $\tau' \in [0, \tau(z_0)]$ from $P(\tau = 0) = 0$ consistently with the equation (52) to obtain $P(\tau(z_0))$ and $\tau(z_0)$.

Initial conditions for the dimensionless flux and mass are just $\sigma(\zeta = 0) = 0$, $q(\zeta = 0) = 1$. The additional condition is following from the symmetry of the system about the equator:

$$q(\zeta = 1) = 0. \tag{55}$$

Now, we solve the system (48) as the initial value problem with the parameter z_0 and vary z_0 to satisfy the condition (55).

The solution of the system (48) is shown at the figure 8. The structure was calculated in the assumptions of Kramers or Thompson opacity. We conclude that the exact form of the opacity is unimportant for the vertical distribution of *dimensionless* parameters. To be completely honest, nothing (opacity, inclination χ, model of magnetic field) is important for the vertical structure. It is almost independent on everything.

Now in would be nice to calculate the vertical structure with the extreme parameters of accretion and neutron star, say, $\dot{M} = 10^{17} g/s$ and $\mu = 10^{30} G \cdot cm^3$ and with the same frequency $f = 200 Hz$. We were able to do it. Results are displayed at the figure 9

7 RADIAL STRUCTURE

Ketsaris & Shakura introduced parameters $\Pi_{1\ldots4}$ which (in their approach) are to be determined after the boundary-condition problem is solved. These parameters are:

$$\begin{cases} \Pi_1 = \frac{\Omega_k^2 z_0^2 \mu}{\Re T_c}, \\ \Pi_2 = \frac{\Sigma_c}{2z_0\rho_c}, \\ \Pi_3 = \frac{\alpha\Re T_c \Sigma_c}{W_{r\phi}\mu}, \\ \Pi_4 = \frac{3}{32}\left(\frac{T_{eff}}{T_c}\right)^4 \frac{\Sigma_c\kappa_0\rho_c^{\iota}}{T_c^{\gamma+4}}. \end{cases} \tag{56}$$

Values denoted as 'c' are evaluated in the centre of the disk. These parameters can be calculated in our approach as well. Combinations of these parameters are basically the coefficients in **order-of-magnitude** formulas for the parameters of the disk. Π_1-parameter is also needed for the viscosity coefficient, and, thus, for the magnetic field. All these parameters are weak functions of the accretion rate. The system (56) is essentially the system of algebraic equations for central temperature and pressure, surface density, relative half-thickness of the disk. Let us introduce $f(r)$:

$$W_{r\varphi}(r) = -\frac{\dot{M}\Omega_k(r)}{2\pi}f(r). \tag{57}$$

and some additional parameters (see Suleimanov et al. (2007) for the investigation of their behaviour):

$$\begin{cases} \Pi_z = (\Pi_1^{19}\Pi_2^{-2}\Pi_3^4\Pi_4^{-2})^{1/40} \approx 2.6, \\ \Pi_\Sigma = (\Pi_1^1\Pi_2^2\Pi_3^{16}\Pi_4^2)^{1/20} \approx 1.03, \\ \Pi_T = (\Pi_1^{-1}\Pi_2^{-2}\Pi_3^4\Pi_4^{-2})^{1/20} \approx 1.09. \end{cases} \tag{58}$$

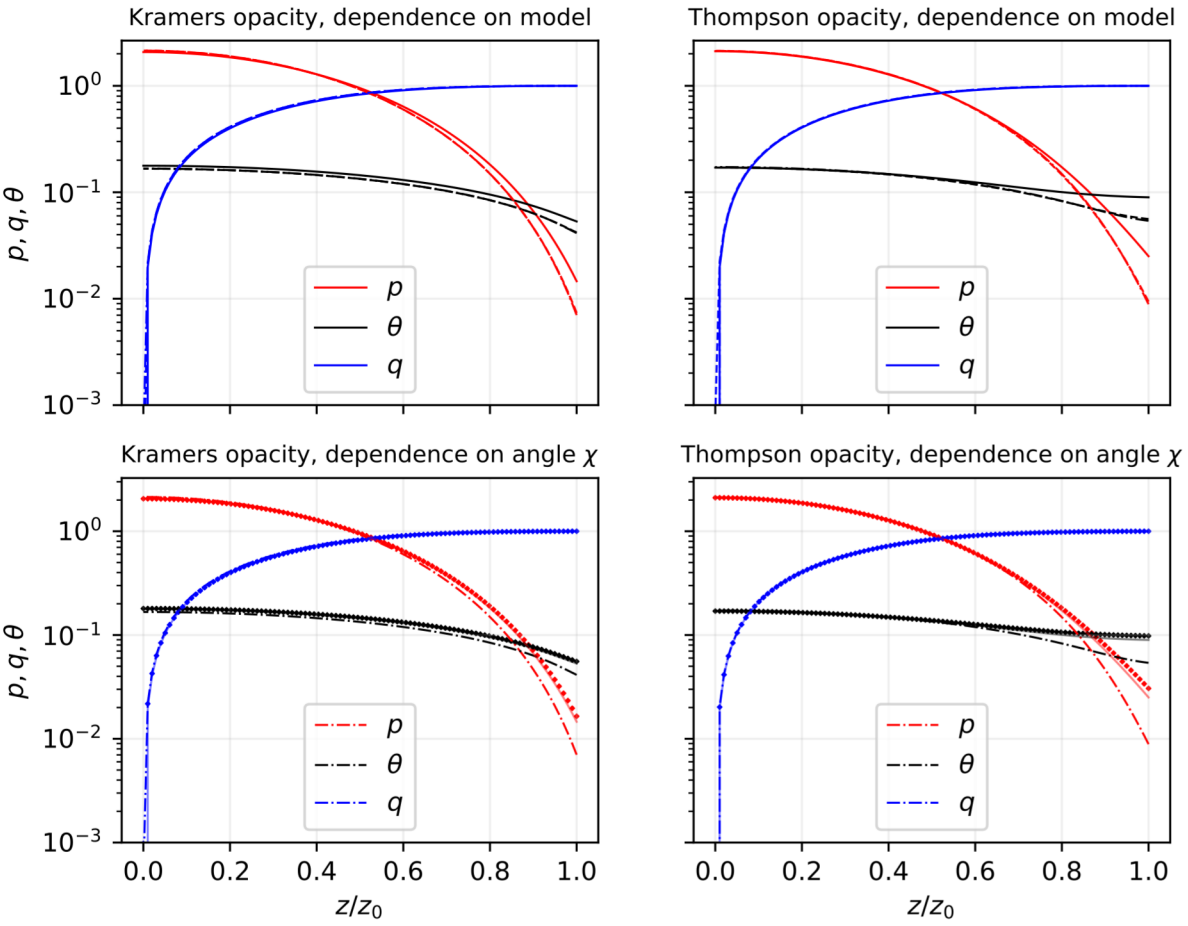

Figure 8. Distribution of dimensionless parameters of the disk (pressure, temperature, radiative flux) over the vertical coordinate. In left (right) column the Kramers (Thompson) opacity is taken. In the top row the dependence on the model is shown. Solid line corresponds to standard disk case, dashed line corresponds to the reconnection model of induced field, dash-dotted line — to our model of the magnetic field. In the low row only our model of magnetic field is adopted, inclination angles $\chi = 0°$ (dash-dotted line) and $\chi = 90°$ (scattering) are shown. Note that only near-surface regions of the disk are sufficiently alternated by model of opacity, inclination angle, model of magnetic field. The interiors of the disk are almost indifferent to all assumptions about the disk or magnetic field. Standard non-magnetic model is also shown for the reference at the bottom two figures as pale solid curves. $\dot{M} = 10^{13} g/s$, $\mu = 10^{26} G \cdot cm^3$.

Then from the system (56) we find:

$$\begin{cases} z_0/r = 0.007 M_{1.4}^{-3/8} \dot{M}_{17}^{3/20} \alpha^{-1/10} r_7^{1/8} f(r)^{3/20} \Pi_z, \\ \Sigma_c = 6.3 \cdot 10^3 M_{1.4}^{1/4} \dot{M}_{17}^{7/10} \alpha^{-4/5} r_7^{-3/4} f(r)^{7/10} \Pi_\Sigma, \\ T_c = 7.7 \cdot 10^6 M_{1.4}^{1/4} \dot{M}_{17}^{3/10} \alpha^{-1/5} r_7^{-3/4} f(r)^{3/10} \Pi_T. \end{cases} \quad (59)$$

Thus we can calculate the vertical structure on each radius. We will know the Π-parameters and the thickness of he disk z_0 for each radius. Using (59), we can calculate any other parameter inside the disk. The results, relative half-thickness z_0/r, surface density Σ_c and the temperature in the equatorial plane are shown at the figure 10 (for different models of the induced magnetic field, $\chi = 0°$) and at thefigure 11 (for different χ, our model for the field is adopted).

8 DISCUSSION

In the present paper we considered the effects of the magnetic field of a central star on a disk assuming that magnetic field can penetrate the disk. The purpose of this paper was to estimate how the vertical structure changes if one includes the magnetic field into consideration and how the presence of the magnetic field modifies the radial structure. The calculation of the vertical structure is important for our understanding of whether the disk can exist at the distances significantly closer than the Alfven radius. We proved that the disk can exist at such distances even when the effects of the magnetic field in the stress tensor are bigger than these of matter.

In section 3 we, being unable to get satisfaction from the already existed models of induced magnetic field, properly derived the induction equation for the azimutal magnetic field. Then we found a way to solve it without complex 3-d simulations: assuming thinness and quasi-stationarity of the disk, there is no need for them since this equation can be reduced to the system of ordinary differential

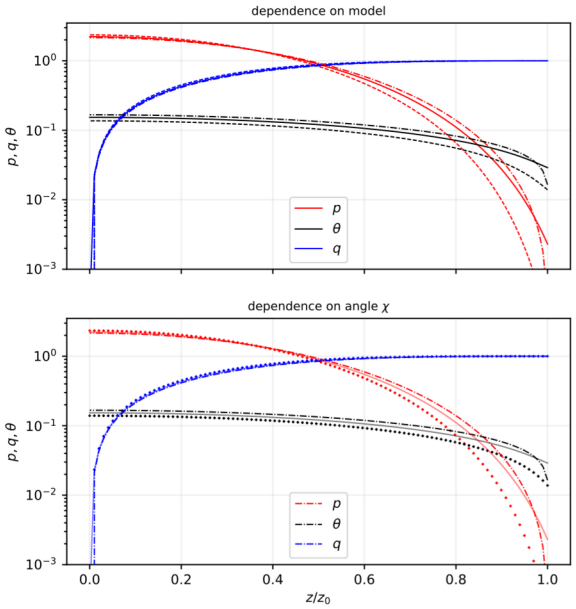

Figure 9. The same as at the fig. 8, but with only Kramers opacity and $\mu = 10^{30} G \cdot cm^3$, $\dot{M} = 10^{17} g/s$.

equations with boundary conditions. Even though the formula for the induced field onto the surface of the disk looks similar to the one obtained in Wang (1995) (Wang (1997) for the case of an inclined rotator), we demonstrated that there are φ-dependent components of the induced field that should be considered. The magnetic field inside the disk is shown to depend on semi-thickness of the disk $h(r) = z_0(r)/r$ and on parameter Π_1 (see sections 3 and 6). This means that the equations of magnetic field structure and disk structure should be solved self-consistently.

In section 4 we derived the equation for the inner radius r_0 of the viscous accretion disk. Results are compared with the model with r_0 being an Alfven radius r_a. Results are close to the ones already obtained in KR07 (in the case on inclination angle $\chi = 0$) and in Wang (1995), Wang (1997), Bozzo et al. (2018). We then derived an expression for the viscous stress tensor $W_{r\varphi}$. Comparison with the standard disk formula shows that the magnetic field can significantly modify stress tensor. In section 5 we demonstrate the possibility for a strong magnetic field to change the spectra of the accretion disk. The intermediate asymptotic $F_\nu \propto \nu^{5/7}$ for the strong magnetic field (or weak accretion) reminds the result obtained in Siuniaev & Shakura (1977) for the disks without an accretion onto the central object ("dead disks").

In section 6 the vertical structure of the disk is calculated using equations of hydromagnetic equilibrium. It is clear that the distributions of parameters inside the disk (like a gas pressure, temperature, the energy flux) normalized to the corresponding values in the disk equator are not sufficiently modified by the magnetic field. We were able to calculate the vertical structure for the parameters $\mu = 10^{30} G \cdot cm^3$, $\dot{M} = 10^{17} g/s$. This can be understood as the possibility of existence of accretion disks around highly magnetized stars. Such systems may be observed as an ULXS.

In opposite, the absolute values of the parameters of the disk may considerably depend on the magnetic field. We calculate the radial distributions of some important disk parameters in the section 7. When the relative importance of the magnetic field is rather small, the energy release rate decreases with increasing magnetic field due to the increasing inner radius of the viscous disk. But if the accretion rate decreases considerably (or, one can imagine that the magnetic field is somehow became stronger), disk can become brighter than the one without the magnetic field.

ACKNOWLEDGEMENTS

DATA AVAILABILITY

REFERENCES

Bozzo E., Ascenzi S., Ducci L., Papitto A., Burderi L., Stella L., 2018, A&A, 617, A126

Campbell C. G., 1992, Geophysical and Astrophysical Fluid Dynamics, 63, 179

Campbell C. G., 2010, MNRAS, 403, 1339

Campbell C. G., Heptinstall P. M., 1998a, MNRAS, 299, 31

Campbell C. G., Heptinstall P. M., 1998b, MNRAS, 301, 558

Ghosh P., Lamb F. K., 1979a, ApJ, 232, 259

Ghosh P., Lamb F. K., 1979b, ApJ, 234, 296

Ghosh P., Lamb F. K., Pethick C. J., 1977, ApJ, 217, 578

Kato S., Fukue J., Mineshige S., 2008, Black-Hole Accretion Disks — Towards a New Paradigm —, 549 pages, including 12 Chapters, 9 Appendices, ISBN 978-4-87698-740-5, Kyoto University Press (Kyoto, Japan), 2008., -1

Ketsaris N. A., Shakura N. I., 1998, Astronomical and Astrophysical Transactions, 15, 193

Kluźniak W., Rappaport S., 2007, ApJ, 671, 1990

Lipunova G., Malanchev K., Shakura N., 2018, in Shakura N., ed., Astrophysics and Space Science Library Vol. 454, Astrophysics and Space Science Library. p. 1, doi:10.1007/978-3-319-93009-1_1

Lovelace R. V. E., Romanova M. M., Bisnovatyi-Kogan G. S., 1995, MNRAS, 275, 244

Revnivtsev M., Churazov E., Postnov K., Tsygankov S., 2009, A&A, 507, 1211

Siuniaev R. A., Shakura N. I., 1977, Pisma v Astronomicheskii Zhurnal, 3, 262

Suleimanov V. F., Lipunova G. V., Shakura N. I., 2007, Astronomy Reports, 51, 549

Wang Y. M., 1987, A&A, 183, 257

Wang Y. M., 1995, ApJ, 449, L153

Wang Y. M., 1997, ApJ, 475, L135

Zel'dovich Y. B., Shakura N. I., 1969, Soviet Ast., 13, 175

APPENDIX A: DERIVATION OF THE INDUCTION EQUATION

We will start from the equation (19) without the first term:

$$\frac{\partial \vec{B}}{\partial t} = \mathrm{rot}\left[\vec{v} \times \vec{B}\right] + \eta_T \Delta \vec{B} + \left[\frac{\mathrm{grad}\eta_T}{\eta_T} \times [\vec{v} \times \vec{B}]\right]. \quad \text{(A1)}$$

The components of the dipole field are obtained easily **??????**:

$$\vec{B}_d = \frac{\mu}{(r^2+z^2)^{5/2}}[(2r^2 \sin\chi\cos\varphi + 3rz\cos\chi - z^2\sin\chi\cos\varphi)\vec{e}_r + \\ + (\sin\chi\sin\varphi(r^2+z^2))\vec{e}_\varphi + \\ + (-r^2\cos\chi + 3rz\sin\chi\cos\varphi + 2z^2\cos\chi)\vec{e}_z]. \quad \text{(A2)}$$

Even though the monstosity of this expression beckons us to neglect all the terms proportional to z (since $h = z/r \ll 1$), we should

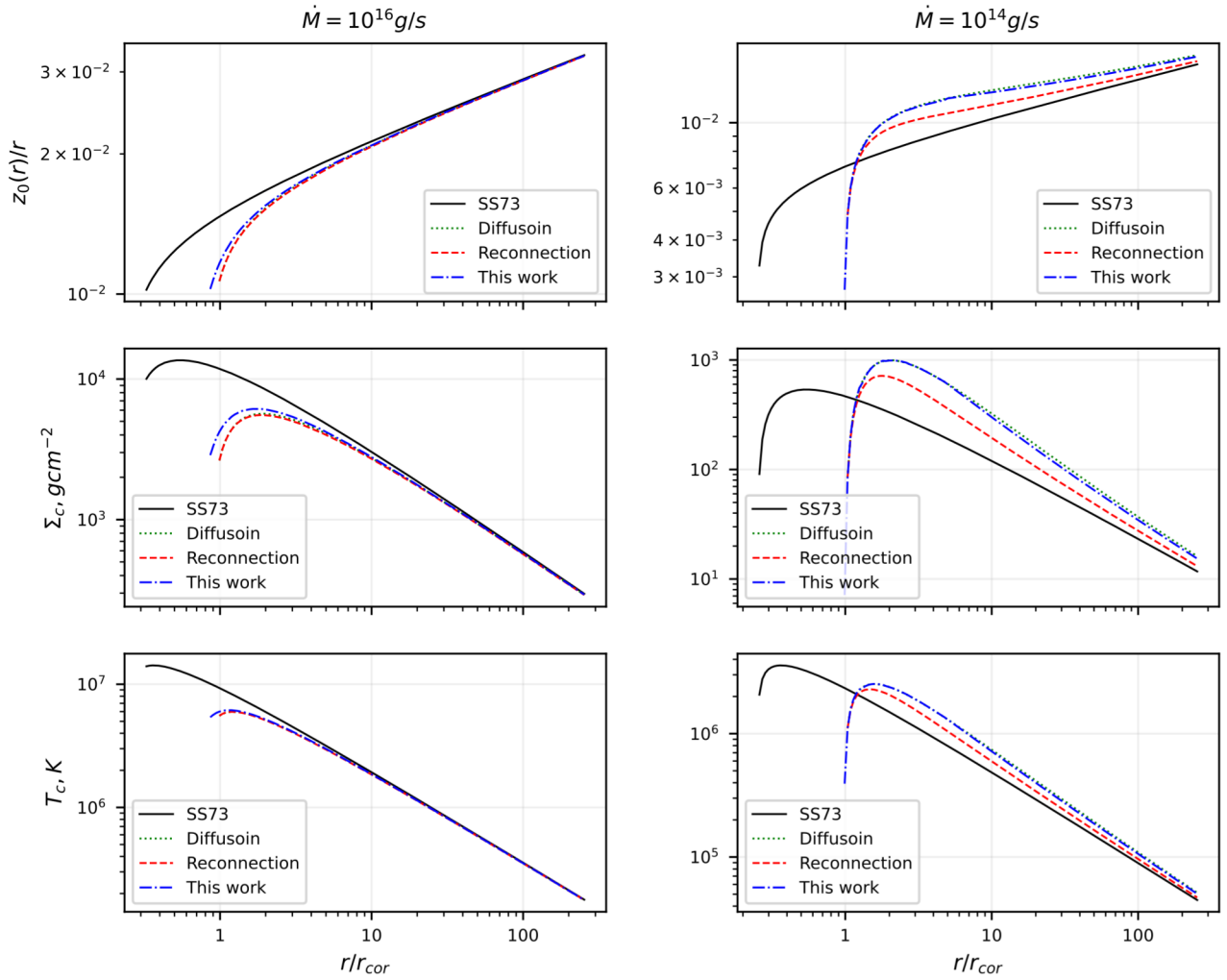

Figure 10. Radial distributions of parameters of the disk: relative half-thickness z_0/r, central surface density Σ_c and central temperature T_c. Different models of the induced magnetic field are displayed. Inclination angle $\chi = 0$ everywhere.

not do it. In this paper we want to obtain all our formulas with the accuracy of $O(h)$ neglecting the terms h^2, h^3..., but since magnetic field is in the equations in non-trivial ways (for example, in second z derivative), all terms in (A2) will contribute in final expression.

Then we use:

$$\mathrm{rot}\left[\vec{v}\times\vec{B}\right] = -\frac{V}{r}\frac{\partial B_r}{\partial\varphi}\vec{e}_r + \vec{e}_\varphi\left(\frac{\partial(VB_z)}{\partial z} + \frac{\partial(VB_r)}{\partial r}\right). \tag{A3}$$

The last term in the (A1):

$$\left[\frac{\mathrm{grad}\eta_T}{\eta_T}\times[\vec{v}\times\vec{B}]\right] = \frac{1}{2r}\left[\vec{e}_r\times[\vec{v}\times\vec{B}]\right] = \vec{e}_\varphi\frac{VB_r}{2r}. \tag{A4}$$

The Laplace operator for the vector field in the cylindrical coordinates:

$$\Delta\vec{B} = \left(\Delta B_r - \frac{B_r}{r^2} - \frac{2}{r^2}\frac{\partial B_r}{\partial\varphi}\right)\vec{e}_r + \left(\Delta B_\varphi - \frac{B_\varphi}{r^2} + \frac{2}{r^2}\frac{\partial B_\varphi}{\partial\varphi}\right)\vec{e}_\varphi + \Delta B_z\vec{e}_z \tag{A5}$$

If the vector field is quasi-stationary than **Beskin???**:

$$\frac{\partial\vec{A}}{\partial t} = \Omega_s\left(\frac{\partial A_r}{\partial\varphi}\vec{e}_r + \frac{\partial A_\varphi}{\partial\varphi}\vec{e}_\varphi + \frac{\partial A_z}{\partial\varphi}\vec{e}_z\right). \tag{A6}$$

In that case three components of the induction equation are:

$$\begin{cases} \Omega_s\dfrac{\partial B_r}{\partial\varphi} = -\dfrac{V}{r}\dfrac{\partial B_r}{\partial\varphi} + \eta\left(\Delta B_r - \dfrac{B_r}{r^2} - \dfrac{2}{r^2}\dfrac{\partial B_r}{\partial\varphi}\right), \\ \Omega_s\dfrac{\partial(B_{\varphi 0}+b_\varphi)}{\partial\varphi} = \dfrac{\partial(VB_z)}{\partial z} + \dfrac{\partial(VB_r)}{\partial r} + \dfrac{VB_r}{2r} + \\ +\eta\left(\Delta B_\varphi - \dfrac{B_\varphi}{r^2}\dfrac{2}{r^2}\dfrac{\partial B_\varphi}{\partial\varphi}\right), \\ \Omega_s\dfrac{\partial B_z}{\partial\varphi} = \eta\Delta B_z = 0. \end{cases} \tag{A7}$$

It has already been said that in our model the matter moves with

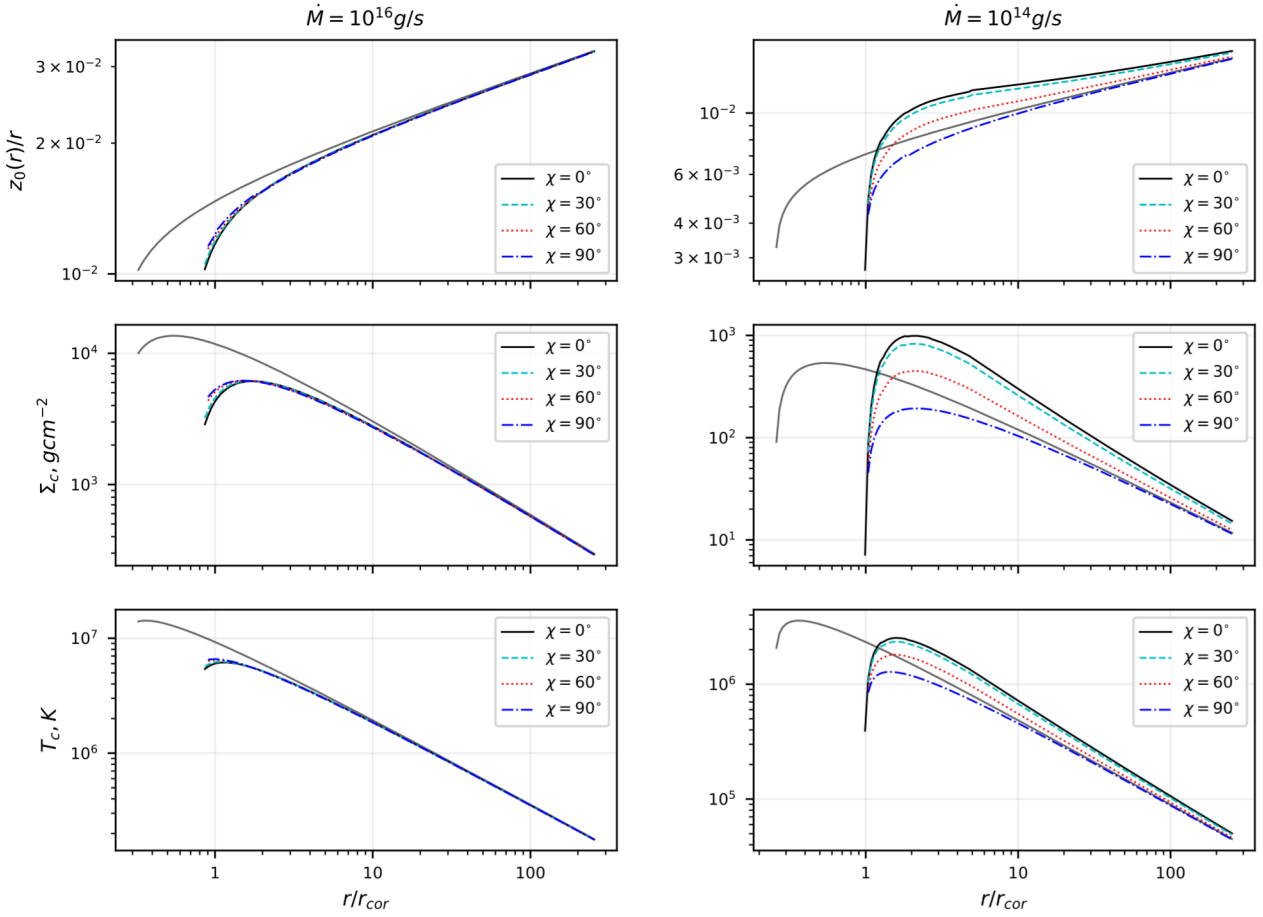

Figure 11. Radial distributions of parameters of the disk: relative half-thickness z_0/r, central surface density Σ_c and central temperature T_c. Different inclination angles χ are shown. The model of magnetic field is this work model. Standard disk case is also present as pale gray curves.

a Keplerian velocity within the disk and corotates with NS angular velocity without the disk. Thus,

$$\frac{\partial V}{\partial r} = \frac{V}{r}\left\{\begin{array}{ll} -1/2 & \text{disk,} \\ 1 & \text{magnetosphere.}\end{array}\right\} + \Omega_s r_0 \frac{1-\omega}{\omega}\delta(r-r_0), \quad \text{(A8)}$$

$$\frac{\partial V}{\partial z} = (V_m(r) - V_d(r))(\delta(z-z_0) - \delta(z+z_0)). \quad \text{(A9)}$$

In our model there are only one (azimuthal) non-trivial component of induced magnetic field. Using (17), we finally get (watch out for your eyes!):

$$\Omega_s r \frac{\mu}{r^4}\sin\chi\cos\varphi + \Omega_s \frac{\partial b_\varphi}{\partial\varphi} = V\frac{3\mu}{r^4}(\sin\chi\cos\varphi + 3z/r\cos\chi) +$$
$$+\frac{\mu}{r^3}(-\cos\chi + 3z/r\sin\chi\cos\varphi)(V_m(r) - V_d(r))[\delta(z-z_0) - \delta(z+z_0)] -$$
$$-\frac{\mu V}{r^4}\left\{\begin{array}{ll} 7\sin\chi\cos\varphi + \frac{27}{2}\frac{z}{r}\cos\chi, & \text{disk,} \\ 4\sin\chi\cos\varphi + 9\frac{z}{r}\cos\chi, & \text{magnetosphere.}\end{array}\right\} +$$
$$\Omega_s r_0 \frac{1-\omega}{\omega}\frac{\mu}{r^3}(2\sin\chi\cos\varphi + 3z/r\cos\chi)\delta(r-r_0) +$$
$$+\frac{V\mu}{r^3}\left\{\begin{array}{ll} 1/2r, & \text{disk,} \\ \nabla\eta_T/\eta_T (= \mathbf{0?} = \mathbf{1/2r?}) & \text{magnetosphere.}\end{array}\right\} \times$$
$$\times (2\sin\chi\cos\varphi + 3z/r\cos\chi) +$$
$$+\eta_T\left(\frac{2\mu\sin\chi}{r^5}(2\sin\varphi + \cos\varphi) + L[b_\varphi]\right). \quad \text{(A10)}$$

Here operator $L[F]$ is:

$$L[F] = \frac{1}{r}\frac{\partial}{\partial r}\left(r\frac{\partial F}{\partial r}\right) + \frac{1}{r^2}\frac{\partial^2 F}{\partial\varphi^2} + \frac{\partial^2 F}{\partial z^2} - \frac{F}{r^2} + \frac{2}{r^2}\frac{\partial F}{\partial\varphi}. \quad \text{(A11)}$$

.

First of all, there are only terms proportional to $1, \cos\varphi$ or $\sin\varphi$ in this equation. This means that the induced field also should satisfy this rule. This looks awful, but now we need only the components of the induced magnetic field not dependent on φ. For $b = b(r, z)$ inside the disk we get the equation:

$$\frac{1}{r}\frac{\partial}{\partial r}\left(r\frac{\partial b}{\partial r}\right) - \frac{b}{r^2} + \frac{\partial^2 b}{\partial z^2} = 3\mu\sqrt{GM}\cos\chi\frac{z}{\eta_T r^{11/2}}. \tag{A12}$$

Using the formulas for the magnetic diffusivity (21) and (22), we come to the first equation in (24). Now we integrate (A10) over $[z_0 - \varepsilon, z_0 + \varepsilon]$, with $\varepsilon \ll z_0$. Assuming $\eta_T^{\text{magnetosphere}} \gg \eta_T^{\text{disk}}$ we obtain the boundary condition on the surface of the disk:

$$\left.\frac{\partial b}{\partial z}\right|_{z=z_0} = -\frac{C}{2}\left(1 - \frac{\Omega_s}{\Omega_k}\right)\frac{1}{r^4}. \tag{A13}$$

We remind that $C = 3\Pi_1\mu\cos\chi/2\alpha h^2\epsilon_d$. This expression contains unknown parameter ϵ_d. It was explained in the main text why we require $C = 2\mu\cos\chi/h_0$. This implies $\epsilon_d = 3\Pi_1/4\alpha h$.

The boundary condition on the lower surface of the disk is obtained in exactly the same way. The boundary condition on the inner radius of the disk can be found similarly:

$$\left.\frac{\partial b}{\partial r}\right|_{r=r_0} = -\frac{3C(1-\omega)}{2}\frac{1}{r_0^4}\frac{z}{r_0}. \tag{A14}$$

The system of equations for b_1, b_2 with boundary conditions can be derived from (A10) as well. Since all the calculations are the same as before, we give the final system:

$$\begin{cases}
\frac{1}{r}\frac{\partial}{\partial r}\left(r\frac{\partial b_1}{\partial r}\right) + 2\frac{b_2 - b_1}{r^2} - \frac{2}{h_0 r^2}\left(\frac{r}{r_c}\right)^{3/2} b_2 + \frac{\partial^2 b_1}{\partial z^2} = f_1, \\
\frac{1}{r}\frac{\partial}{\partial r}\left(r\frac{\partial b_2}{\partial r}\right) - 2\frac{b_2 + b_1}{r^2} + \frac{2}{h_0 r^2}\left(\frac{r}{r_c}\right)^{3/2} b_1 + \frac{\partial^2 b_2}{\partial z^2} = f_2, \\
\left.\frac{\partial b_1}{\partial z}\right|_{z=z_0} = \left.\frac{\partial b_1}{\partial z}\right|_{z=-z_0} = g_z, \\
\left.\frac{\partial b_1}{\partial z}\right|_{z=z_0} = \left.\frac{\partial b_1}{\partial z}\right|_{z=-z_0} = 0, \\
\left.\frac{\partial b_1}{\partial r}\right|_{r=r_0} = g_r, \\
\left.\frac{\partial b_1}{\partial r}\right|_{r=r_0} = 0, \\
b_1(r = r_l) = b_2(r = r_l) = 0.
\end{cases} \tag{A15}$$

Here right-hand sides are:

$$\begin{cases}
f_1 = \frac{2\mu\sin\chi}{r^5}\left(\frac{3}{h_0} - 1 + \frac{1}{h_0}\left(\frac{r}{r_c}\right)^{3/2}\right), \\
f_2 = -\frac{4\mu\sin\chi}{r^5}, \\
g_z = \frac{3\mu\sin\chi}{r^4}\left(\left(\frac{r}{r_c}\right)^{3/2} - 1\right), \\
g_r = -2\mu\sin\chi\frac{1-\omega}{h_0 r_0^4}.
\end{cases} \tag{A16}$$

What we want to do next is to make a substitution to **reset conditions** along z-axis:

$$\begin{cases}
b_1 = \beta_1 + g_z \cdot z, \\
b_2 = \beta_2.
\end{cases} \tag{A17}$$

and expand the solution in the series in terms of eigenfunctions of the Sturm-Liouville problem (27).

APPENDIX B: ANALYTICAL SOLUTION FOR THE INDUCTION EQUATION

Let us take the problem (26) and turn our variables into dimensionless ones. We normalize β to the vertical dipole field: $\beta \to \beta \cdot \mu\cos\chi/r_c^3$. The distance is measured in units of corotation radius: $r \to r \cdot r_c$. Assuming that relative half-thickness of the disk $h_0 = z_0(r)/r$ changes only slightly over the wide range of distances, we write $z_0/r_c = h_0 = \text{const}$. Then, vertical coordinate is in units of the half-thickness of the disk: $z = h_0 r \cdot x$. With these changes:

$$\begin{cases}
\frac{1}{r}\frac{\partial}{\partial r}\left(r\frac{\partial\beta}{\partial r}\right) - \frac{\beta}{r^2} + \frac{1}{h_0^2 r^2}\frac{\partial^2\beta}{\partial x^2} = 6\frac{x}{r^6}\left(7r^{3/2}/8 - 3/2\right), \\
\beta(x = 0) = 0, \\
\left.\frac{\partial\beta}{\partial x}\right|_{x=1} = 0, \\
\left.\frac{\partial\beta}{\partial r}\right|_{r=\omega^{2/3}} = \frac{1 + \omega/2}{\omega^{8/3}}x, \\
\beta(r = a) = \frac{a^{3/2} - 1}{a^3}x.
\end{cases} \tag{B1}$$

All the boundary conditions and the right-hand side of the equation are anti-symmetric functions of x. This means that β is also anti-symmetric function of x. Notice that this is not true for the $b_1(r, z)$ and $b_2(r, z)$. We consider the problem on the interval $[0, 1]$ instead of $[-1, 1]$ by changing the boundary condition at the lower surface to the boundary condition at the equator: $\beta(x = 0) = 0$ due to anti-symmetry. Now let's find the solution in form

$$\beta(r, x) = \sum_{n=0}^{\infty}\sin(\mu_n x)B_n(r). \tag{B2}$$

For the coefficients $B_n(r)$ we obtain 1-dimensional boundary condition problem (BC problem). Using linearity of all equations here, we divide B into sum of two problems: $B(r) = u(r) + v(r)$. The problem for u includes all zero BC but non-zero right hand side of the equation. In opposite, the problem for v has trivial right hand side of the equation but non-zero BC:

$$\begin{cases}
\frac{1}{r}(ru')' - \frac{M_n^2 u}{r^2} = f(r), \\
u'(\omega^{2/3}) = 0, \\
u(a) = 0, \\
f(r) = 6\frac{(-1)^n}{\mu_n^2}\frac{1}{r^6}\left(\frac{7r^{3/2}}{4} - 3\right).
\end{cases} \tag{B3}$$

$$\begin{cases} \dfrac{1}{r}(rv')' - \dfrac{M_n^2 v}{r^2} = 0, \\ v'(\omega^{2/3}) = 2\dfrac{(-1)^n}{\mu_n^2}\dfrac{1+\omega/2}{\omega^{8/3}}, \\ v(a) = 2\dfrac{a^{3/2}-1}{a^3}. \end{cases} \tag{B4}$$

Here $M_n^2 = 1 + \mu_n^2/h_0^2$. This step is necessary for the analytical solving of the equation, but actually it is faster and easier to solve the problem numerically for the acceptable number of n-s just for the $B_n(r)$ without any further preparations. For example, we do not know the analytical solution for the b_1, b_2, and we find these components using expansion (B2) and solving 1-d BC problem for the coefficients.

Anyway, the analytical solutions are important since they give the opportunity to test our codes and they are beautiful sometimes.

The problem for v has the solution:

$$v(r) = Ar^M + Br^{-M}, \tag{B5}$$

and coefficients A, B are to be found from the boudary conditions. This is just simple mathematics, so we will not stop here.

The problem for u can be solved in the following way. We solve the Sturm-Liuoville problem with the corresponding boundary conditions:

$$\begin{cases} \dfrac{1}{r}(r\tilde{v}')' - \dfrac{M_n^2}{r^2}\tilde{v} + \lambda_m \tilde{y} = 0, \\ +\text{zero BC}. \end{cases} \tag{B6}$$

Eigenfunctions are

$$\tilde{v}_{mn} = J_{M_n}(r\sqrt{\lambda_{mn}}) - N_{M_n}(r\sqrt{\lambda_{mn}}) \cdot \frac{J_{M_n}(a\sqrt{\lambda_{mn}})}{N_{M_n}(a\sqrt{\lambda_{mn}})}, \tag{B7}$$

where eigenvalues are roots of the equation:

$$\frac{J'_{M_n}(\omega^{2/3}\sqrt{\lambda_{mn}})}{J_{M_n}(a\sqrt{\lambda_{mn}})} = \frac{N'_{M_n}(\omega^{2/3}\sqrt{\lambda_{mn}})}{N_{M_n}(a\sqrt{\lambda_{mn}})}. \tag{B8}$$

Then

$$v_n(r) = -\sum_m \frac{f_{mn}}{\lambda_{mn}}\tilde{v}_{mn}(r). \tag{B9}$$

Here

$$f_{mn} = \frac{1}{||\tilde{v}_{mn}||^2}\int_{\omega^{2/3}}^{a} \tilde{v}_{mn} r \mathrm{d}r, \tag{B10}$$

$$||\tilde{v}_{mn}||^2 = \int_{\omega^{2/3}}^{a} r\tilde{v}_{mn}^2 \mathrm{d}r. \tag{B11}$$

This paper has been typeset from a TEX/LATEX file prepared by the author.